OBSERVATION OF THE FRAGMENTATION CLOUD OF THE INTELSAT 33E BREAKUP WITH THE SPACE OBSERVATION RADAR TIRA

D. Cerutti-Maori, C. Carloni, I. Maouloud, S. Mouret, F. Rosebrock, V. Karamanavis, F. Schlichthaber, and J. Schroer

Fraunhofer Institute for High Frequency Physics and Radar Techniques FHR, Fraunhoferstrasse 20, 53343 Wachtberg, Germany, Email: Delphine.Cerutti-Maori@fraunhofer.fhr.de

ABSTRACT

As a consequence of the explosion of Intelsat 33e on October 19, 2024, a significant number of pieces of debris were released in the geostationary orbit, every piece being a potential threat to any active satellite in this orbital region. Even though ground-based radars are not the sensors of choice to detect, monitor, and track GEO fragments due to the long distances between the sensors and the pieces, they can help to characterize GEO fragmentation clouds. Indeed, they can deliver complementary information to optical systems such as range, range rate, and range-rate rate. This paper presents the results of an observation of the fragmentation cloud of Intelsat 33e conducted with the space observation radar TIRA on November 6, 2024. After introducing the developed signal processing scheme, the statistics of the detected fragments are shown, including their size and parameter distributions.

Keywords: Radar, Space debris, GEO.

1. INTRODUCTION

On October 19, 2024, the satellite Intelsat 33e [1, 2] exploded causing several thousand of debris being released in the geostationary orbit [3, 4, 5]. ESA is estimating the number of debris larger than 1 cm to be around 16,000 [6]. As this event could have catastrophic consequences for the active satellites in the geostationary orbit, several ground-based sensors are currently tracking the fragments generated by this breakup.

Although optical systems are the sensors of choice to observe, track, and catalog geostationary pieces of debris, radar systems can also be used to gain complementary insight into fragmentation clouds in this orbital regime. Due to the long ranges involved when observing GEO fragments by ground-based radar, the backscattered signals are very faint and the received signal power is usually below the noise power. Indeed, the Signal-to-Noise Ratio (SNR) for radar systems is inversely proportional to the fourth power of the range, i.e. SNR $\propto \frac{1}{R^4}$, yielding an SNR loss of 64 dB for a GEO space object at a range of 40,000 km compared to a LEO object at a distance of 1,000 km. In order to detect GEO fragments and be able to discriminate between pieces of debris with similar parameters, adapted signal processing techniques based on signal integration have to be applied, as single-pulse detection is inappropriate.

To understand the potential contribution of ground-based radars for characterizing GEO fragmentation clouds, an observation of the Intelsat 33e breakup was performed with the Tracking and Imaging Radar (TIRA) [7] on November 6, 2024. The paper presents the results of the data acquisition. After describing the conducted measurement in Section 2, Section 3 gives an overview of the signal processing scheme developed to detect the fragments and estimate their parameters. In order to assess the size of the detected fragments, different Radar Cross Section (RCS) models were used, which are introduced in Section 4. Section 5 examines the statistics of the parameters of the detected pieces of debris and Section 6 concludes the investigation by discussing the benefits and limitations of ground-based radars when observing GEO breakups.

2. CONDUCTED OBSERVATION

The space observation radar TIRA is equipped with a 34 m parabolic antenna in Cassegrain configuration. The resulting large antenna gain is essential for detecting small fragments at long ranges. Two complementary radars are sharing this antenna, an L band tracking radar and a Ku band imaging radar. Only the tracking radar was used to observe the GEO fragmentation cloud as the radar link budget of the imaging radar is insufficient for detecting objects in the GEO orbital regime.

As mentioned previously, the data acquisition took place on November 6, 2024, approximately three weeks after the breakup. The total duration of the observation was about 16 min. The TLE of a known piece (hereafter "TLE fragment") was used to initialize the measurement. The

Proc. 9th European Conference on Space Debris, Bonn, Germany, 1–4 April 2025, published by the ESA Space Debris Office
Editors: S. Lemmens, T. Flohrer & F. Schmitz, (http://conference.sdo.esoc.esa.int, April 2025)

Table 1. TLE data set of a known fragment used to trigger the measurement

1	XXXXXU	80951	24301.72130368	-.00000001	00000-0	00000+0	0	44
2	XXXXX	0.0417	150.7673	0023258	112.6914	96.3016	1.00378857	93

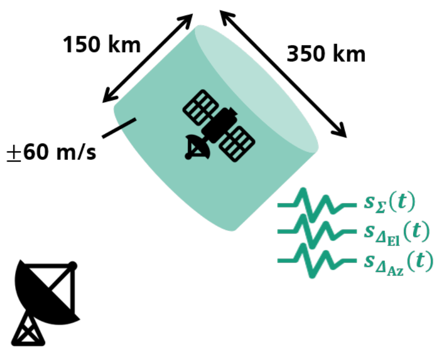

Figure 1. Observation scheme

TLE data set is listed in Table 1. An unmodulated pulse of a length of 1 ms was transmitted with a Pulse Repetition Frequency (PRF) of about 30 Hz. The resulting range resolution was 150 km and the range rate resolution 115 m/s. The antenna footprint is 350 km at a range of 40,000 km. Figure 1 illustrates the data acquisition geometry. A cylinder with a diameter of 350 km and a length of 150 km was monitored over time to detect the fragments with a radial velocity within the interval ±60 m/s, which crossed this volume. Three signals, which were output by the monopulse system, were recorded simultaneously: the sum signal $s_\Sigma(t)$ and the difference signals in elevation $s_{\Delta_{\rm El}}(t)$ and in azimuth $s_{\Delta_{\rm Az}}(t)$.

A major difference between the observation of a breakup event in the LEO and GEO orbital regimes is the dwell time of the fragments. While a piece of debris crosses the TIRA antenna beam in a few seconds in LEO [8], it can remain visible for several hours/days in GEO. On the one hand, the longer visibility time improves the target detection performance. On the other hand, it complicates the clustering of the single detections to one single tracklet, as explained in the next section.

3. RADAR SIGNAL PROCESSING

The signal transmitted by a ground-based radar, backscattered by a GEO object, and received by a ground-based receiver is usually very faint and below the noise level. For this reason, the signal has to be integrated over several pulses to increase the SNR and enable target detection. A coherent integration was selected for the present investigation as it increases the integration gain by a factor of about $\sqrt{N}$ compared to an incoherent integration, with N being the number of integrated pulses.

The Coherent Processing Interval (CPI), which is directly proportional to the number of pulses N, plays a major role in the detection performance. Longer integration times reduce the minimum detectable fragment size. However, the decorrelation caused by the system phase instability and the object motion (translational and rotational motion) strongly increases with the processing time. These decorrelation effects deteriorate the impulse response by raising its sidelobe levels and broadening its main lobe. Different integration intervals were examined to find the best trade-off between signal decorrelation and integration gain. A CPI of about 7 s was chosen for subsequent processing.

Several coherent filters can be used. To account for different relative motions between the fragments and the radar, a Matched Filter (MF) bank was applied in the range rate and range-rate rate dimensions, as introduced in [9]. To do this, the complex receive signal $s_\Sigma(t)$ was correlated with the signal expected for an object moving with a given relative range rate and range-rate rate. The tested range rate and range-rate rate parameters were chosen within a specific interval of values. This processing allows to separate fragments, which are located simultaneously within the antenna beam and within the main lobe of the ambiguity function, as illustrated in Figure 2. Two objects with different relative motions can be clearly identified after matched filtering. Due to the low PRF, very high sidelobes can be observed in the impulse responses. These high sidelobes can hide the signal of faint targets, impeding their detection. In addition, it is important to consider these sidelobes when deriving an appropriate detection threshold to ensure a low number of false alarms.

The same processing was applied to the radar data acquired during the observation of the fragmentation cloud of Intelsat 33e. Figure 3 presents an MF processing result with subsequent detection and preliminary clustering of the single detections. The data in Figure 2 were simulated according to the parameters of the fragments detected in Figure 3. A good agreement can be observed between Figures 2(b) (simulated radar data) and 3(a) (measured radar data). A range-rate rate in the interval [-8, 8] m/s^2 was tested during the MF processing. The detection step is realized by comparing the output of the MF with a threshold. Afterwards, the detections corresponding to the same fragment are grouped together, as shown in Figure 3(b). For each cluster, the corresponding azimuth and elevation angles are computed using the

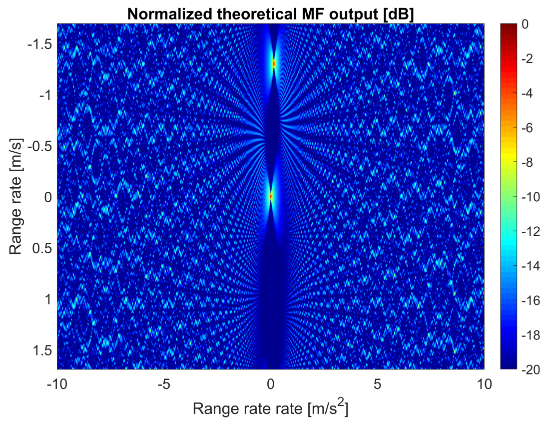

(a) Impulse responses of two objects with equal RCS and different range rate / range-rate rate parameters

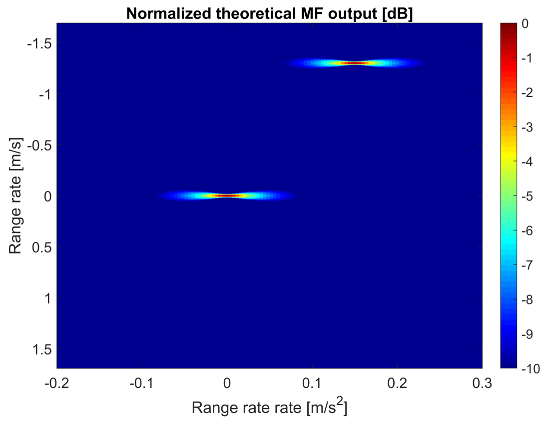

(b) Zoom of Figure 2(a)

Figure 2. Simulated MF response [Object 1 (0 m/s^2,0 m/s), Object 2 (0.15 m/s^2,-1.3 m/s)]

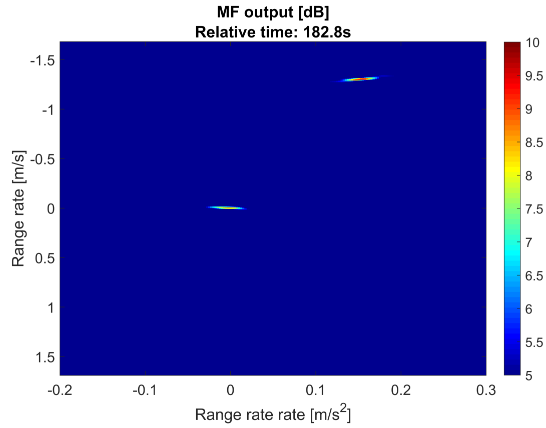

(a) MF processing

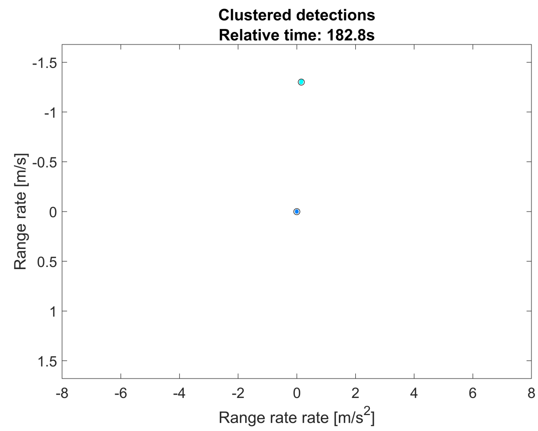

(b) Clustered detections over one data set

Figure 3. MF processing result

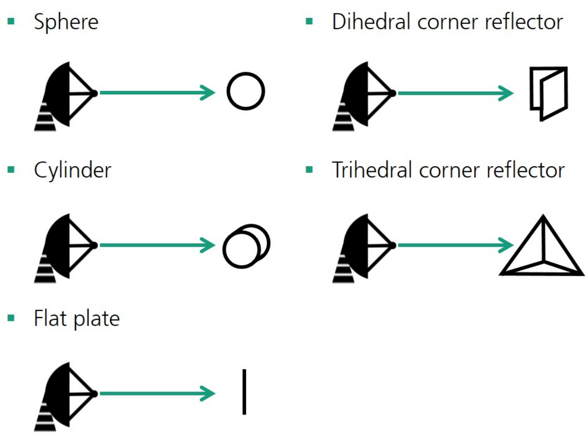

Figure 4. Simple metallic object shapes considered for RCS modeling

monopulse dechirping principle [9], which exploits the ratio between the difference signals $s_{\Delta_{\mathrm{El}}}(t)$ and $s_{\Delta_{\mathrm{Az}}}(t)$ and the sum signal $s_{\Sigma}(t)$. Finally, a second clustering step in the 4D space (range rate, range-rate rate, azimuth angle, elevation angle) is applied to regroup the multiple detections of each identified fragment over time.

4. RCS MODELLING

The RCS of an object depends on a variety of parameters such as its material and shape, the radar frequency, and the polarization of the waves. The incidence angle, i.e. the orientation of the object with respect to the radar, plays also a major role as it impacts the effective surface of the object and the backscattering process. Deriving the physical size of an object from an RCS is unfortunately a complicated task as there is no one-to-one relationship between these two parameters.

Figure 4 presents different shapes of a metallic object, whose RCS have been modeled in Figure 5(a) assuming a backscattering regime in the optical region [10]. The RCS corresponds to the maximum RCS that can be measured over the incidence angle. Indeed, while the RCS is constant for a sphere, it strongly depends on the incidence

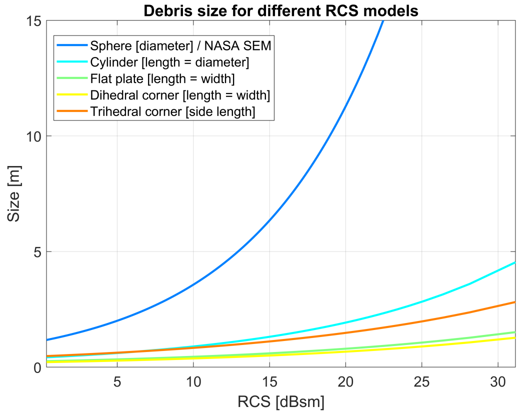

(a) RCS modeling for the different shapes shown in Figure 4

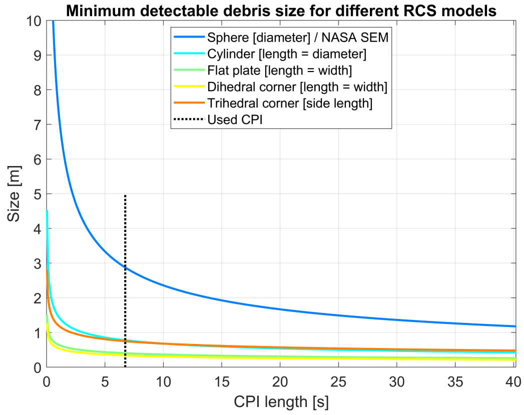

(b) Minimum detectable debris size for different object shapes and CPI lengths

Figure 5. RCS modeling and minimum detectable object size for the TIRA system

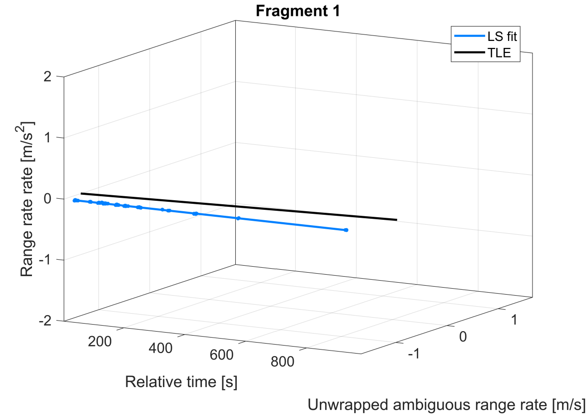

(a) Range-rate rate and range rate over detection time with corresponding data fit

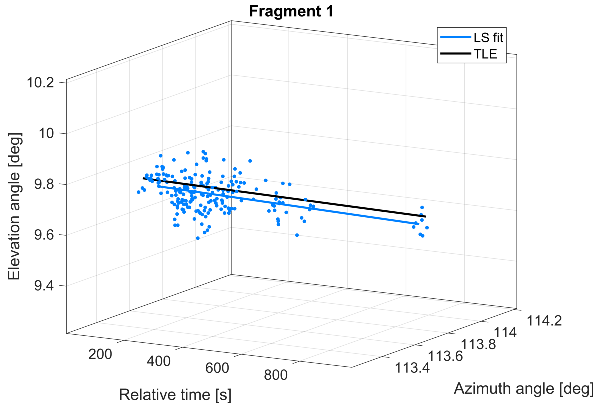

(b) Azimuth and elevation angles over detection time with corresponding data fit

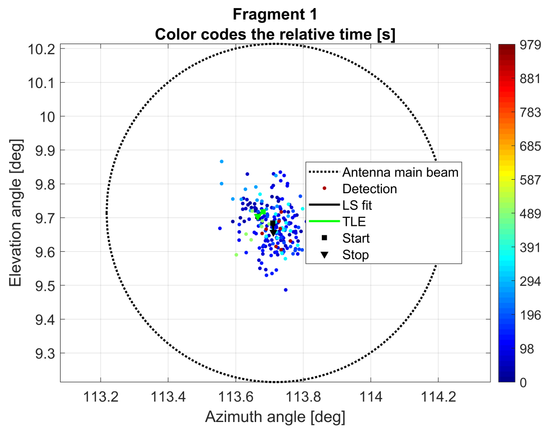

(c) Beam crossing direction

Figure 6. Parameters of the TLE fragment

angle for a flat plate for example. We assumed geometric shapes of unit aspect ratio (e.g. a cylinder whose diameter is equal to its length and a plate whose width is equal to its length). One observes that the RCS of a sphere is much smaller compared to the RCS of the other object shapes. This raises the question of modeling the shape of a fragment. While very small fragments of a few centimeters in size can be reasonably modeled by a sphere, it is questionable if this modeling applies to larger fragments of around 1 m in size. As a consequence, several RCS models should be used for larger fragments to roughly derive lower and upper bounds for their dimensions. It has to be mentioned that additional parameters such as the incidence angle and the material, which also impact the RCS, were not considered in the RCS modeling of Figure 5.

The minimum detectable object size can be derived for the different object shapes and the parameters of the TIRA system according to the integration length. The selected CPI length of about 7 s is represented by the dashed line in Figure 5(b), where we can see that fragments of around 40-50 cm in size should be detectable in GEO.

5. DETECTED FRAGMENTS

This section presents the statistics of the detected fragments. While Section 5.1 concentrates on the TLE fragment (see Table 1) for validating the developed processing scheme, the other sections examine the parameter dis-

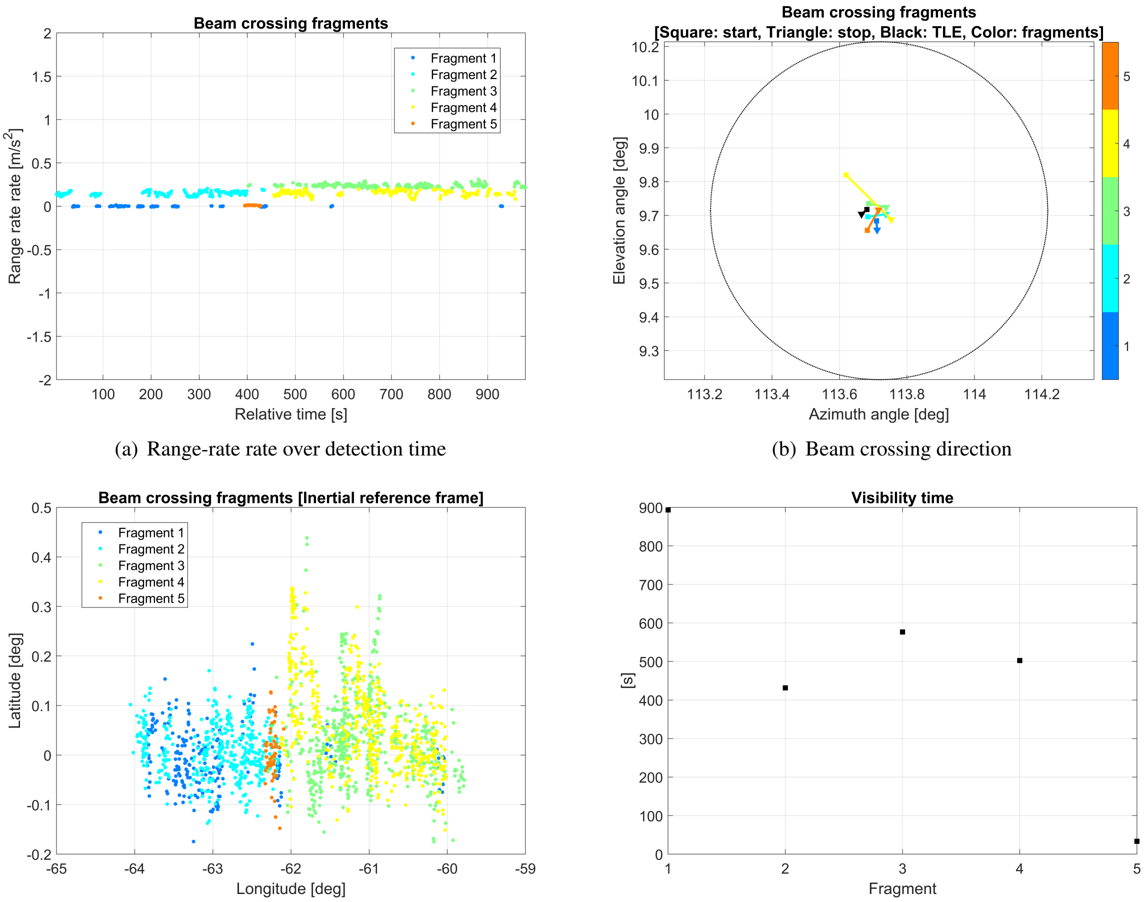

(a) Range-rate rate over detection time

(b) Beam crossing direction

(c) Estimated latitude and longitude

(d) Visibility time

Figure 7. Parameters of the detected fragments

tributions of all the detected pieces of debris.

5.1. TLE fragment

The TLE fragment could be identified in the detection list by correlating its expected parameters with the parameters of the detected fragments. Figure 6 shows the measured parameters of the TLE fragment over time. The black lines in Figures 6(a) and 6(b) indicate the expected parameters of the fragment, which were derived after propagating the TLE data set. A good agreement can be observed for the four measured parameters (i.e. range-rate rate, range rate, azimuth angle, and elevation angle). As the quality of the TLE data set is unknown, only a qualitative comparison can be done. Note that the measured range rate can be ambiguous due to the low PRF. Although the range rate can be unwrapped over time using proper data clustering, it still remains ambiguous. The beam crossing direction can be estimated from the azimuth and elevation angles using a weighted Least Square (LS) fit. Figure 6(c) exhibits that the estimated beam crossing direction of the TLE fragment (black line) is consistent with the one derived from the TLE data set (green line).

5.2. Detected fragments

Figure 7 presents the estimated parameters of the detected fragments. Fragment 1 in Figure 7 corresponds to the TLE fragment introduced in the previous section. Five different fragments were detected during the observation, all with a range-rate rate in the interval [0, 0.3] m/s^2. As mentioned previously, the tested range-rate rate interval was between -8 and 8 m/s^2. No debris with large range-rate rates were detected. Figure 7(a) reveals that the range-rate rate of a fragment is nearly constant over time. Furthermore, Figure 7(b) indicates that the detected pieces of debris crossed the average antenna beam around its center. In Figure 7(c), the estimated latitudes and longitudes of the fragments over time are plotted in an Earth-Centered inertial reference frame (as opposed to the Earth-Centered Earth-Fixed (ECEF) reference frame where the longitudes of the fragments would be around 67.5 deg). The low estimation accuracy observed for a single estimate is caused by the low SNR. Indeed, the estimation accuracy is inversely proportional to the square

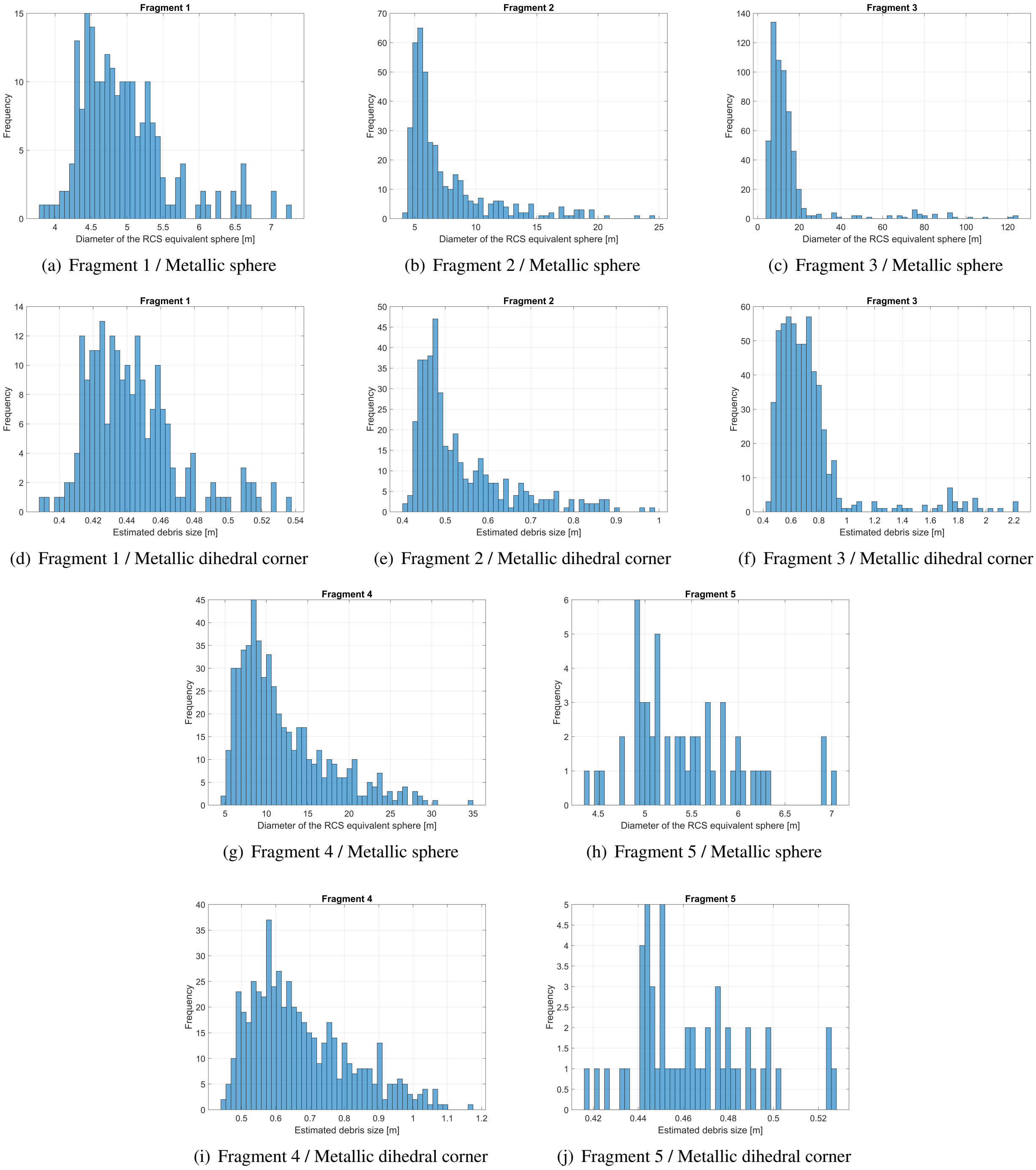

(a) Fragment 1 / Metallic sphere
(b) Fragment 2 / Metallic sphere
(c) Fragment 3 / Metallic sphere
(d) Fragment 1 / Metallic dihedral corner
(e) Fragment 2 / Metallic dihedral corner
(f) Fragment 3 / Metallic dihedral corner
(g) Fragment 4 / Metallic sphere
(h) Fragment 5 / Metallic sphere
(i) Fragment 4 / Metallic dihedral corner
(j) Fragment 5 / Metallic dihedral corner

Figure 8. Estimated fragment size using different RCS models

root of the SNR. As the visibility time of GEO objects is longer compared to LEO objects, this parameter can be exploited to increase the overall estimation accuracy by combining all the temporal detections in an adapted weighted LS model. As expected and evidenced in Figure 7(d), each fragment has a different visibility time. It can be explained by the fact that the pieces of debris have to be simultaneously in the antenna beam and in the same range/Doppler cell after pulse compression to be detected[1]. As shown by the simulation of the breakup

[1]As previously mentioned, this fact is a limitation of the current tracking radar system. The TIRA system is currently being upgraded [7]. In the upcoming development stage, it will be possible to transmit user-defined waveforms, sample several range cells, and compress the data according to a wide range of expected Doppler shifts (single pulse processing prior to coherent (or incoherent) processing over several pulses). This will strongly improve the system performance as it will allow the detection of fragments over a large range-Doppler region.

modeled as a high energy explosion in [5], the pieces of debris present a wide range of different perigee/apogee combinations, implying that the debris will not cross the antenna beam in the same range cell. The visibility time is therefore different from the antenna beam crossing time.

5.3. Estimated fragment size

Figures 8 and 9 present the lower and upper bounds of the debris size according to the RCS models introduced in Section 4. Assuming that a fragment has the same probability of having one of the five shapes shown in Figure 4, its size should lie between the lower and upper bounds shown in Figure 8, with a strong tendency to be closer to the lower bound according to the modeling of Figure 5. Figure 9 reveals that the estimated object size derived from the measured RCS of a single detection is strongly varying over time for Fragments 2-5. This indicates that these fragments are tumbling and that their shapes cannot be modeled as a sphere. In contrast, a smoother tumbling motion may be inferred from the less fluctuating estimated size of Fragment 1. Taking the average of the size distributions in Figure 8 yields a rough estimate of the fragment size. All debris should be around 50-60 cm in size.

5.4. Estimated orbital parameters

Figure 10 shows the estimated orbital parameters of the first four fragments. The visibility time of Fragment 5 is too short for reasonably assessing its orbital elements. The estimated orbital periods (Figure 10(a)), inclinations (Figure 10(b)), and semi-major axes (Figure 10(c)) are plausible according to the breakup modelings presented in [5, 6]. The orbital period and the semi-major axis were estimated under the assumption of a circular orbit as a first approximation.

5.5. Correlation with the TLE catalogue

To ensure that the clustered detections correspond to newly created GEO fragments from the breakup of Intelsat 33e and not to already known objects or active satellites, the previous detection list was correlated with the elements contained in the TLE catalogue. One finds that INSAT 1A (NORAD ID: 13129) entered the edge of the antenna beam during the last minute of the observation. However, it crossed the beam in another range cell than the one being tested and thus remained undetected for this data acquisition setting.

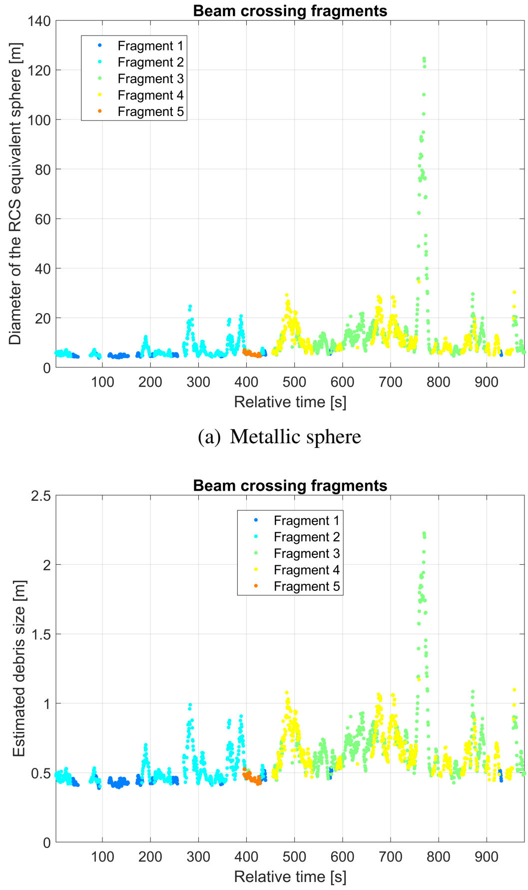

(a) Metallic sphere

(b) Metallic dihedral corner

Figure 9. Estimated fragment size over time

6. CONCLUSION

This paper presented the results of an observation of the fragmentation cloud of Intelsat 33e with the space observation radar TIRA. A total number of 5 pieces of debris were detected over an observation time of about 16 min. Different RCS models were used to evaluate the dimension of the fragments from the measured RCS. The analysis revealed that all the debris should have a size around 50-60 cm. Their orbital parameters were also derived and found to be within the range of possible values estimated by breakup modelings found in the literature.

Additional observations are required to extrapolate the number of fragments and confirm other sources. As no assumption about the spatial distribution of the debris (e.g. uniform distribution) can be made from this single observation, the number of fragments could not be assessed.

The present investigation showed that radar systems can add valuable information during the characterization of breakup events in the geostationary orbit. Although they are not as sensitive as optical systems due to the long

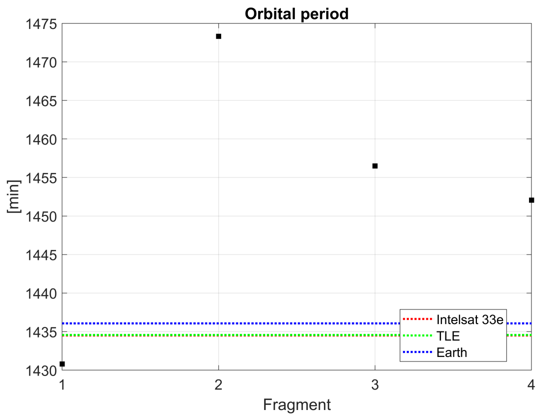

(a) Orbital period

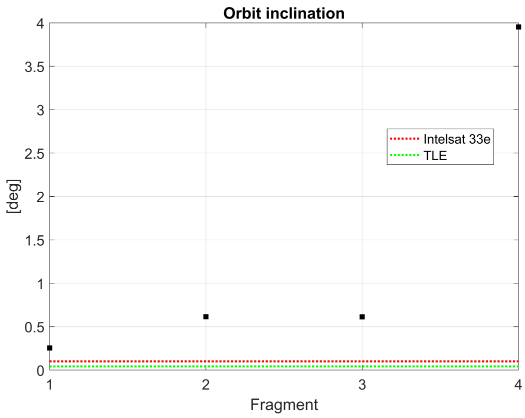

(b) Orbit inclination

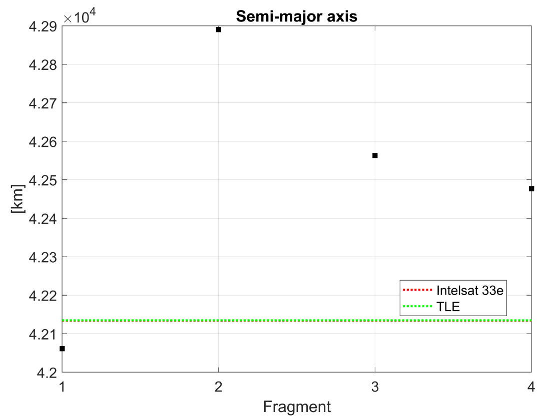

(c) Semi-major axis

Figure 10. Estimated orbital parameters

distances between the GEO fragments and the ground-based radars, they provide additional parameters such as the range, the range rate, and the range-rate rate of the measured debris. These ranging data fused with the angular information of optical systems could improve orbit determination. In addition, the physical size of the fragments and their attitude motion (e.g. tumbling behavior) could be better appraised from the combined RCS and light curve measurements [11].

ACKNOWLEDGMENTS

The present study has been jointly financed by the German Space Situational Awareness Center (GSSAC) and the European Space Operations Centre (ESOC).

REFERENCES

1. https://space.skyrocket.de/doc_sdat/intelsat-33e.htm
2. https://www.n2yo.com/satellite/?s=41748
3. https://www.datacenterdynamics.com/en/news/500-pieces-of-debris-from-intelsat-33e-now-being-tracked/
4. https://spacenews.com/exoanalytic-observes-500-pieces-of-debris-from-intelsat-33e-breakup/
5. https://www.okapiorbits.space/blog-events/intelsat-33e-break-up-a-closer-look
6. https://fragmentation.esoc.esa.int/home/blog/intelsat-33e-fragmentation
7. J. Klare et al., *The Future of Radar Space Observation in Europe - Major Upgrade of the Tracking and Imaging Radar (TIRA)*, Remote Sens. 2024, 16(22), 4197, https://doi.org/10.3390/rs16224197
8. D. Cerutti-Maori, C. Carloni, J. Rosebrock, and J Siminski, *Observation of COSMOS-1408 Debris Cloud with the Tracking and Imaging Radar (TIRA) System*, Proc. 2nd NEO and Debris Detection Conference, Darmstadt, Germany, 2023
9. D. Cerutti-Maori, J. Rosebrock, C. Carloni, M. Budoni, I. Maouloud, and J. Klare, *A novel high-precision observation mode for the tracking and imaging radar TIRA - principle and performance evaluation*, Proc. 8th European Conference on Space Debris, Darmstadt, Germany, 2021
10. Merill I. Skolnik, *Radar Handbook*, McGraw-Hill Professional
11. A. Vananti, D. Kucharski, M. Steindorfer, R. Kanzler, P. Kärräng, D. Cerutti-Maori, J. Rosebrock, and T. Schildknecht, *Multi-sensor space object tracking for tumbling motion characterization*, Proc. 2nd NEO and Debris Detection Conference, Darmstadt, Germany, 2023